forum acusticum 2026
8-12 September · Graz, Austria

SECONDARY SOURCE METHOD FOR POLYGONAL SCATTERING OBJECTS WITH CAVITIES

U. Peter Svensson[1], Anders Langørgen[1], Magne Skålevik[2]

[1] *Acoustics group, Department of Electronic Systems, Norwegian University of Science and Technology, Norway*
[2] *Brekke & Strand AS, Oslo, Norway*

Abstract

A tube ending in an infinite baffle is a classical radiation problem and has been studied extensively, with closed-form or semi-analytical results for radiation impedance, directivity, and end correction. In contrast, an unflanged tube introduces additional physics, such as edge diffraction, making analytical treatment more challenging. This problem is highly relevant for simulating musical instruments based on resonances in tubes. Here, secondary sources are used to couple the interior and exterior domains of a partially open shoebox. Green's functions between all secondary-source pairs are needed for both domains under rigid-walled boundary conditions. For the interior, a modal solution is used, while the exterior domain is modeled with an edge-diffraction integral-equation formulation. A rectangular tube with one open end and inner dimensions 10 cm × 10 cm × 60 cm was investigated. Measurements were made in an anechoic chamber, with a microphone placed near the bottom corner inside the tube and a tweeter loudspeaker positioned 2 m from the opening. The ratio of microphone pressure amplitudes was measured with the box present and in an otherwise identical free-field setup. The same scenario was simulated in MATLAB. Measurements and simulations generally agree quite well for the first six axial resonances. The Q-factor of the first few resonances were underestimated by the simulation, likely due to loss mechanisms that were not represented in the simulation.

Keywords: *Scattering, open cavities, coupled problems.*

1. Introduction

Open cavities are quite common structures in outdoor sound propagation, ranging from large scale cases such as courtyards, to smaller scales such as various balcony constructions. At the extreme end of such a complexity scale, open pipes/tubes/ducts can be viewed as open cavities. A common approach for analysing such problems has been to divide the domain into an interior subdomain and an exterior one [1]. The inner subdomain can be a shoebox-shaped, or cylindrical, cavity for which analytical modal expressions are available, whereas more complex interior shapes might require Finite-Element Modeling or other numerical methods. For the exterior subdomain, the infinite baffle has commonly been used because the solution can be easily and accurately computed with the Rayleigh integral [1]. By matching the sound field at the interface between the subdomains, a complete solution can be computed and this has been done for balconies [2], music instruments [3], complex machinery [1]. Often, a more realistic model of the outer subdomain would be a finite object but the computation of the sound field around finite scattering objects has required computationally expensive methods such as BEM, or analytically more complex methods [4]. Here, a similar subdomain-based method will be used, applying an edge-diffraction-based calculation method for the outer subdomain. In this study, a short duct, open at one end, is chosen as a case. Measurements are carried out in an anechoic room, and corresponding calculations are compared with measurements and available reference results. Parts of this work are presented in the Master thesis of the second author, which is not yet published.

2. Theory

The secondary source method was described in [5], where references were also given to some previous uses of that approach. The method is a semi-analytical method which divides a physical domain into subdomains with geometries such that solutions exist, analytically or numerically. Each interface between subdomains is discretised into elements, typically rectangular, and the particle velocity is assumed to

Corresponding author: *peter.svensson@ntnu.no.*

be constant across each such interface element, called secondary sources in the following. This approach is a variant of the Patch Transfer Function [1], for which the Boundary Element Method was used for external subdomains. They compared that accurate approach to the approximation where an opening into an external subdomain was approximated as an opening in an infinite baffle, which can be computed very efficiently with the Rayleigh integral. On the other hand, [1] modeled interior subdomains of complicated geometries and computed the required transfer functions with Finite Element Calculations. In our study, we apply the edge-diffraction based calculation of transfer functions as an efficient and accurate alternative to the boundary element method for the exterior domain [6], and study only interior domains of shoebox-shapes.

2.1. The Secondary Source/Patch Transfer Function formulation

The problem domain is divided into subdomains which are connected via interface surfaces, as illustrated in Figure 1, where a model of an open cavity is shown. The interface surface in Figure 1 is discretized into 9 elements, and the Secondary Source formulation assumes that massless pistons are positioned at the interface, in this case as 3 x 3 secondary sources (SS). The vibration velocities of those SS are the unknowns to compute and they correspond to the particle velocities at the opening of the open cavity. A time-harmonic factor $e^{j\omega t}$ is assumed and suppressed, and then a balance equation is set up in the form of a matrix equation for the soundfield amplitudes for one angular frequency ω,

$$[\mathbf{G}_{\text{in}} + \mathbf{G}_{\text{ext}}]\,\mathbf{v}_{\text{SS}} = \mathbf{p}_{\text{excitation}} \tag{1}$$

where $\mathbf{v}_{\text{SS}} \in \mathbb{C}^{N_{\text{SS}}\times 1}$ stores the N_{SS} unknown SS vibration velocity amplitudes for one angular frequency, $\mathbf{p}_{\text{excitation}} \in \mathbb{C}^{N_{\text{SS}}\times 1}$ stores the excitation sound pressure amplitudes generated by a primary source, at the secondary source locations when these are considered rigid. The primary source is a monopole at location $\mathbf{x}_0$ with source strength Q_0, and then $\mathbf{p}_{\text{excitation}}$ for SS location number j is

$$p_{\text{excitation},j} = H_{\text{SS},j\leftarrow\mathbf{x}_0} Q_0 \tag{2}$$

The matrices $\mathbf{G} \in \mathbb{C}^{N_{\text{SS}}\times N_{\text{SS}}}$ contain all the transfer functions from one SS, in the form of a piston, to the center point of all the N_{SS} secondary sources (including itself). Two $\mathbf{G}$-matrices are needed since the two sides of the SS interface will be different physical subdomains. Again, the transfer functions in the $\mathbf{G}$-matrices should be those for the case when the subdomain interface is considered as rigid, and a single SS acts as a piston. The matrix equation in Eq. (1) can be solved via a matrix inversion, assuming that an inverse is computable. Once the SS vibration amplitudes have been computed, their contributions to a receiver point are computed,

$$p_{\text{sec.,R}} = \mathbf{g}_{\text{R}\leftarrow\text{SS}}\mathbf{v}_{\text{SS}} \tag{3}$$

where $\mathbf{g}_{\text{R}\leftarrow\text{SS}} \in \mathbb{C}^{1\times N_{\text{SS}}}$ stores the N_{SS} transfer functions from the piston SS to a single receiver point R. The final sound pressure at the receiver is a sum of the contributions by the primary source and the secondary sources,

$$\begin{aligned} p_{\text{R}} = p_{\text{prim.,R}} + p_{\text{sec.,R}} &= H_{\text{R}\leftarrow\mathbf{x}_0} Q_0 \\ + \mathbf{g}_{\text{R}\leftarrow\text{SS}}\mathbf{v}_{\text{SS}} &= H^{\text{total}}_{\text{R}\leftarrow\mathbf{x}_0} Q_0 \end{aligned} \tag{4}$$

Here it can be noted that if the primary source and the receiver are in different subdomains, then $H_{\text{R}\leftarrow\mathbf{x}_0} = 0$. Two computational details need to be considered. A first is that the particle velocity in an aperture will have a singularity along the edge of the aperture [7]. This singularity affects the convergence rate for the final solution as the number of SS in the aperture is increased. A second computational detail is that Eq. (1) will imply that a high SS velocity occurs when the combined effect of $\mathbf{G}_{\text{in}}$ and $\mathbf{G}_{\text{ext}}$ has a low amplitude. The values of $\mathbf{G}_{\text{in}}$ are typically computed with a modal formulation for the sound field. In order to get a high accuracy for frequencies where the elements in $\mathbf{G}_{\text{in}}$ have a low amplitude, it will be necessary to include very large numbers of modes.

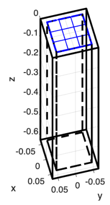

Figure 1: Illustration of an open cavity with an interior subdomain and an exterior subdomain connected via an interface with 3 x 3 secondary sources.

2.2. Transfer Functions for exterior domains

This study is limited to exterior subdomains that are shaped as convex polyhedra, since the chosen numerical method, the diffraction-based Edge Source Integral Equation (ESIE), applies only to convex polyhedra. For details of the ESIE method, the reader is referred to [8], [9]. The transfer functions denoted H in Eqs. (2) and (4) are decomposed into three parts,

$$H_{\mathbf{x}_{\text{R}}\leftarrow\mathbf{x}_0} = H_{\text{GA}} + H_{\text{diff.1}} + H_{\text{HOD}} \tag{5}$$

where H_{GA} is the Geometrical Acoustics solution = direct sound + specular reflection, $H_{\text{diff.1}}$ is first-order diffraction, which is computed by numerical evaluation of a diffraction integral for all edges that are visible from the source and receiver [10], and H_{HOD} is Higher-Order Diffraction (= sum of second- and higher-order diffraction), which is computed via the

ESIE [8]. The ESIE is a Fredholm integral equation of the second kind, which can be computed with the Nyström method, that is, using Gaussian quadrature, where each edge is discretized into a number of quadrature points, or edge points. A matrix equation is formulated for the unknowns, the edge source amplitudes. This equation is of such huge dimensions that the solution must be computed via the iterative Neumann series approach, where each iteration step corresponds to one more diffraction order. Numerically, the accuracy of H_{HOD} will then depend on the diffraction order, and the quadrature order, that is, the number of Gaussian quadrature points per edge. The computation time for the computation of H_{HOD} grows linearly with diffraction order (from order 3), and is $\propto n_{\mathrm{G}}^3$ for the quadrature order per edge, n_{G} [9].

The transfer functions $\mathbf{g}_{\mathrm{R}\leftarrow\mathrm{SS}}$ for the exterior side in Eq. (4) assume a piston source rather than the monopole source that was used in derivations of first- and higher-order diffraction. The GA-term in Eq. (5) becomes a Rayleigh integral computation rather than the explicit e^{-jkr}/r monopole expression. The first- and higher-order diffraction can be computed with some low-order quadrature, representing the piston source with a few monopole sources.

2.3. Transfer Functions for interior domains

For the interior side, this study is limited to cuboid or shoebox-shaped rooms, for which classical modal solutions are available. The details will not be given here, as they are readily available in many sources [11]. In the same way as for the exterior domain, the transfer functions $\mathbf{g}_{\mathrm{R}\leftarrow\mathrm{SS}}$ in Eq. (4) assume a piston source in the interior domain, not a point source which is used in most references. The piston source expression was given in [5] and it is a small extension of the classical point-source modal sum. The modal sum must be truncated and the truncation criterion can be expressed as how many times higher than the frequency of interest is the lowest excluded mode resonance frequency, as a "safety factor". As mentioned above, Eq. (1) leads to that the SS velocity amplitude, $\mathbf{v}_{\mathrm{SS}}$, gets highest when the sum of the transfer function matrices, $\mathbf{G}_{\mathrm{in}} + \mathbf{G}_{\mathrm{ext}}$, is small. For the interior sound field, $\mathbf{G}_{\mathrm{in}}$ is small *between* resonance peaks, and between the resonance peaks, a large number of terms in the modal sum will be needed.

2.3.1. Modeling loss in interior domains

Each term in the modal sum for the interior domains has a denominator which for the lossless case is $\omega_{\mathrm{N}}^2 - \omega^2$, where ω_{N} is the eigenvalue, the resonance angular frequency, of mode $\mathrm{N} = [n_x, n_y, n_z]$. A common way to introduce some kind of loss into the lossless expressions is to define a complex eigenvalue $\omega_{\mathrm{N}} = \omega_{\mathrm{N,R}} + j\delta_{\mathrm{N}}$, but maintain the eigenfunctions/mode functions. Then the δ_{N} will represent the losses that exist in reality, as an approximation. We know some loss mechanisms that occur in practice in an open-cavity case with hard walls:

1. Radiation loss at the opening of the cavity
2. Thermal and viscous boundary losses
3. Losses inside the wall materials during wall vibrations
4. Losses via radiation/transmission, caused by wall vibrations (secondary radiation loss)
5. Air dissipation

In this study, we choose a case with an open cavity constructed with quite rigid and smooth walls, and it is at first assumed that the radiation loss at the opening of the cavity will dominate the losses. It should be noted that the radiation loss will occur when the subdomains are connected, via Eq. (1), but the computation of the transfer functions on the inside of the cavity assume rigid walls. An arbitrarily chosen δ_{N} has to be used for numerical practicalities.

2.4. Axial resonances for open-closed ducts

Open cavities that are substantially higher than they are wide, such as the one illustrated in Fig. 1, will cause axial resonances up to the first frequency were a cross-mode can be generated. The axial resonances, f_n, in open-closed ducts, or pipes, are given by

$$f_n = \frac{2n-1}{4}\frac{c}{L + L_{\text{end corr.}}}, \quad n = [1, 2, 3, ...] \qquad (6)$$

where L is the physical length and the end correction, $L_{\text{end corr.}}$, represents the radiation loss at the opening. Silva et al, [12], gave expressions for the frequency-dependent end corrections of circular pipes, both unflanged and flanged (baffled). The frequency-dependence is often expressed as ka where a is the radius of the cylindrical pipe. The end correction for square pipes, of width W, will be somewhat different but very close to the circular-pipe values if the square-pipe frequency-dependence is expressed as $ka_{\mathrm{eq.}}$ where $a_{\mathrm{eq.}} = W/\sqrt{\pi}$. Values for the end correction of flanged (baffled) and unflanged rectangular pipes have been computed via finite element calculations, [13]. Instead of expressing the end correction, we will here express the "relative shift in resonance frequency" (caused by the end correction), defined as

$$\Delta f_{\mathrm{rel},n} = 100\frac{f_n - \frac{(2n-1)c}{4L}}{\frac{(2n-1)c}{4L}} = 100\left(\frac{4L}{(2n-1)c}f_n - 1\right) \quad [\%] \qquad (7)$$

This expression is easy to interpret when comparing values at different resonances.

3. Case study

3.1. Measurements

An open cavity with inner dimensions 100mm * 100mm * 600 mm was constructed from 15mm thick phenolic film-faced plywood. A half-inch free-field condenser microphone, Brüel & Kjær 4189, was flush mounted through a hole, very close to an inner corner

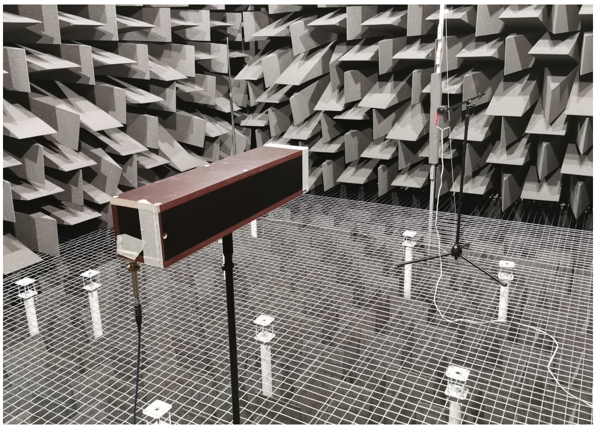

Figure 2: The open cavity used in this study

of the cavity. A small tweeter loudspeaker, a SEAS H1396-04 27TFFNC/G, was used as a sound source, place at a distance of 1.695m from the opening of the cavity, along the extension of the inner edge of the cavity in the long direction; the edge closest to the microphone placement, see Fig. 2. The measurement was then repeated with the microphone placed in the same location relative to the loudspeaker, but without the box. The ratio between those two frequency responses then removed, to a large degree, the influence of the loudspeaker's frequency response.

The measurement software EASERA was used to generate exponential sine sweeps of length 10.9 seconds, with a low enough amplitude that no signs of systematically changing magnitude could be seen during repeated measurements. A sampling frequency of 48 kHz was used, and the impulse responses were windowed to lengths of 8000 samples (167 ms) for the case with the open cavity, and 446 samples (9.3 ms), for the free-field case, respectively. A 100-sample long half-Hann window was applied to the end of the longer impulse responses, before applying an FFT of length 32768.

3.2. Simulations

As indicated in Fig. 1, calculations were done with a subdivision of the portal between the two domains into N by N secondary sources ($N = 3$ in Fig. 1). This way plane waves as well as some first cross modes could be expected to be represented. After some studies of numerical aspects, it was found that including diffraction orders up to 3, and using 16 quadrature points along the longest edges, and 3 along the shorter edges, gave frequency response magnitudes deviating less than 0.3 dB from reference values which were established with a high number of quadrature points and diffraction orders. Simulations with the diffraction order set to 0 gave results for a "baffled" or "flanged" opening of the cavity. Including diffraction instead gave results for the "unflanged" case, which corresponds to the real object, shown in Fig. 2. The simulated results will converge somewhat slowly as the number of secondary sources is increased, because of the singular nature of the particle velocity along the edges in apertures. To study the convergence, some results were computed for increasing numbers of N. Each resonance frequency, and Q-value is then plotted as function of $1/N$ (which is proportional to the side length of the SS pistons), and an empirical convergence rate can be observed, see the Result section. Such a convergence rate facilitates Richardson extrapolation, [6], which uses a few values computed with different grid resolutions (number of SS) to estimate more accurate values via extrapolation.

4. Results and discussion

The measured frequency responses with and without the open cavity in place, respectively, are shown in Fig. 3. They are denoted (output) "spectra" since they include the non-flat source spectrum of the loudspeaker. Also shown is the background noise response, which was estimated by measuring an impulse response without the loudspeaker connected, and by computing the FR with the same kind of windowing as the other FR measurements. It can be seen in Fig. 3 that the signal-to-noise ratio is high down to the first resonance, around 130 Hz, even though a tweeter loudspeaker intended for use above 2 kHz was employed. The division of the two frequency responses removed the influence of the loudspeaker, and this division could then be compared with simulations, as shown in Fig. 4.

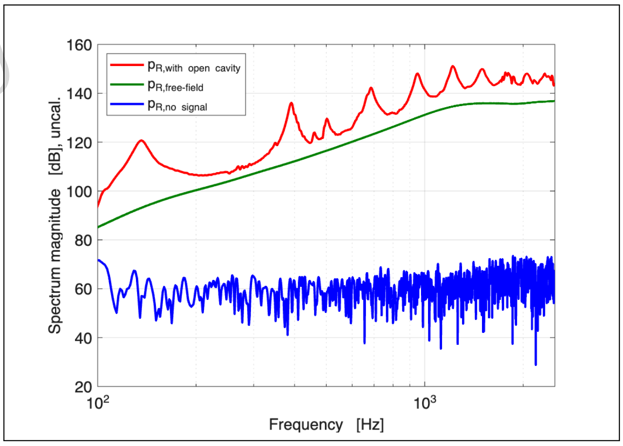

Figure 3: Measured spectra with the open cavity (top), without the open cavity (=free-field, middle), and without excitation signal (corresponding to background noise, bottom curve), respectively.

The frequency responses display the expected axial resonances, at frequencies f_n given by Eq. 6, up to the frequency of the first cross-mode which is around 1715 Hz for the studied case.

Generally, the simulation agrees with the measurements, but the axial resonance frequencies are, after all, easy to estimate quite well. The sharpness of the resonances, or Q-values, are more challenging since they are determined by the amount of radiation loss

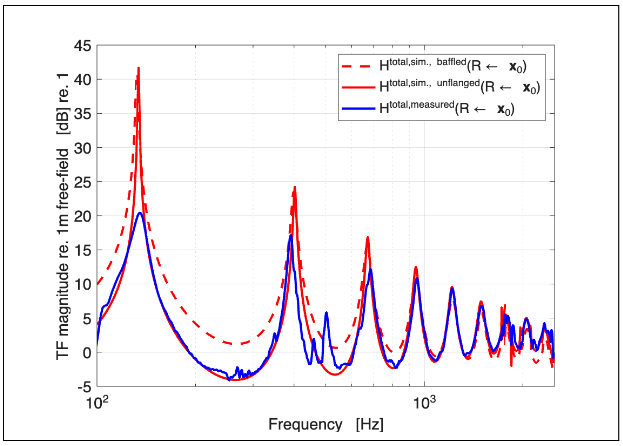

Figure 4: Simulated and measured TFs, $H_{\mathrm{R}\leftarrow x_0}$. Simulated, baffled (red, dashed), simulated, unflanged (red, solid), measured, unflanged (blue, solid).

and other loss mechanisms. The difference between the flanged (baffled) and unflanged simulation results is substantially larger between the resonance peaks than at the resonance peaks, and the unflanged simulation agree much better with the measurements than the flanged simulations do. To inspect more details of the resonances, parameters of the peaks of the frequency response, the resonance frequency and the Q-value, were estimated by fitting a second-order curve to the inverse of the frequency response magnitude squared. The measured response shows a few extra resonances, most prominently around 450 Hz and 500 Hz, which might be caused by resonances of the cavity walls.
As described in section 3.2, the convergence, as function of number of SS, was studied by repeating simulations for different numbers of SS. As one example, Fig. 5 shows the value of the second resonance frequency as function of $1/N$, where N is the number of SS in one dimension. Thus the value of 0.25 on the x-axis shows the value for a 4 x 4 mesh of SS etc. The empirical line fit can then give an improved estimate via the line fit's value for $1/N = 0$: 404.27 Hz. The same extrapolation procedure was used for the Q-values.
Fig. 6 shows the experimental, theoretical, and simulated resonance frequencies in terms of relative shift of each resonance frequency, as given by Eq. 7. The theoretical values are from [13], where values for square ducts were given. First, the simulated results for the baffled/flanged case agree very well with the theoretical values, using end corrections from [13]. For the unflanged case, the simulations differ from the theoretical values and it is unclear how much of this is caused by the small difference in wall thickness. The details of the simulations might need further investigations. The measured results show quite much variation and it is not really possible to draw any conclusion about the fit between theoretical/simulated results and simulations. As a sidenote, it can be acknowledged that the unflanged and flanged/baffled cases agree more and more the higher the frequency, which indicates that for higher frequencies it might suffice to use an assumption of a baffled case.
Fig. 7 shows the Q-values and it can be observed that the first resonance had a much lower Q-value in the experiments than in the simulations. For resonances number 4-6, the simulated unflanged case gives results that are quite similar to the measured ones, and for resonances 2-3 the simulated values (again, for the unflanged case) are also substantially higher than the measured values. For the three lowest resonances, there might be substantial amounts of non-radiation losses in the measurements, such as thermal/viscous boundary losses, but such losses are ignored in the simulations here. A trend like this could be expected since radiation losses increase with increasing frequency whereas boundary losses have a less steep frequency dependence [3]. Further experiments and/or numerical simulations with other methods should be carried out to explore this further.

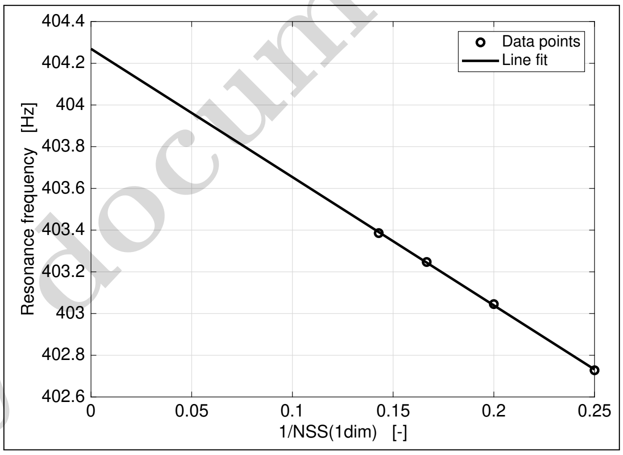

Figure 5: The value of the second resonance frequency computed for 4 different numbers of SS, as function of number of SS in one dimension, and the empirical line fit
.

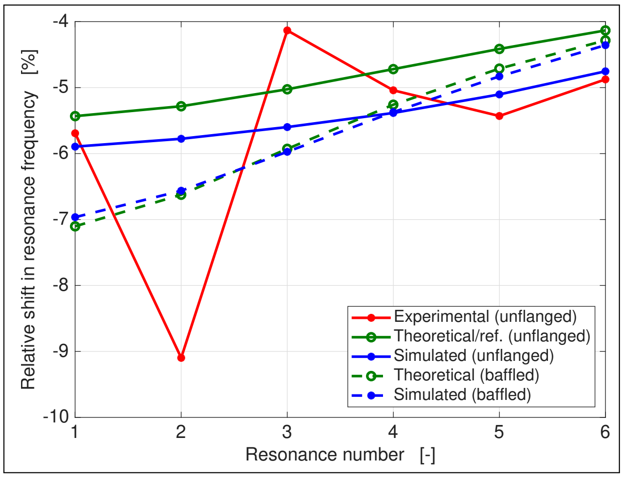

Figure 6: Relative shift in resonance frequency, as defined by Eq. 7.

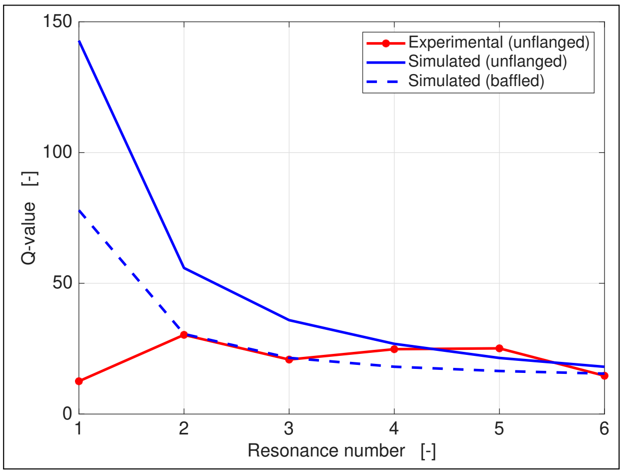

Figure 7: Q-values for the first six resonance peaks in Fig. 4.
.

5. Conclusion

- The simulations gave transfer functions that generally were quite similar to the measurements. Especially between resonance peaks, simulations of an unflanged cavity were much closer to the measured results than simulations of a baffled cavity opening were.

- It was not possible to draw conclusions about the simulations' accuracy resonance frequency estimation since the measurement results displayed a bit of variation. The simulations agreed well with theoretical values for the baffled case but showed some unexplained differences for the unflanged case.

- Systematic differences were observed between measurements and simulations for the Q-values. The measurements showed substantially lower Q-values, that is, higher loss, than the simulations. This indicated that the loss mechanisms mentioned in Section 2.3.1, which are not included in the simulations, probably had significant effect.

- The simulation method seems to work well but is somewhat numerically challenging: interior sound fields will require large numbers of modes, and the interface need to be discretized with a fine resolution if very accurate results are sought. Richardson extrapolation might be used to accelerate the convergence.

6. Acknowledgments

The authors acknowledge getting numerical values from W. Duan for the computed results in [13].

References

[1] M. Ouisse, L. Maxit, C. Cacciolati, and J.-L. Guyader, "Patch transfer functions as a tool to couple linear acoustic problems," *Journal of Vibration and Acoustics*, vol. 127, pp. 458–466, 2005.

[2] W. Kropp and J. Bérillon, "A theoretical model to consider the influence of absorbing surfaces inside the cavity of balconies," *Acustica united w Acta Acustica*, vol. 86, pp. 485–494, 2000.

[3] N. H. Fletcher and T. D. Rossing, *The Physics of Musical Instruments. Second edition.* Springer, 1998.

[4] H. Levine and J. Schwinger, "On the radiation of sound from an unflanged circular pipe," *Physical Review*, vol. 73, pp. 383–406, 1948.

[5] U. P. Svensson, K. H. Reigstad, and M. Skålevik, "Simulation method for shoebox-shaped rooms with absorbing ceilings," in *Proc. of Forum Acusticum Euronoise*, Malaga, Spain, 2025, pp. 4201–4206.

[6] S. R. Martin, U. P. Svensson, J. Schlechta, and J. O. Smith, "Modeling sound scattering using a combination of the edge source integral equation and the boundary element method," *Journal of the Acoustical Society of America*, vol. 144, pp. 131–141, 2018.

[7] D. P. Hewett and U. P. Svensson, "The diffracted dield and its gradient near the edge of a thin screen (l)," *Journal of the Acoustical Society of America*, vol. 134, pp. 4303–4306, 2013.

[8] A. Asheim and U. P. Svensson, "An integral equation formulation for the diffraction from convex plates and polyhedra," *Journal of the Acoustical Society of America*, vol. 133, pp. 3681–3691, 2013.

[9] U. P. Svensson, V. Henriksen, and H. Olsen, "Handling impedance surfaces in diffraction modeling," *Acta Acustica*, vol. 9, 2025, Art. no. 23.

[10] U. P. Svensson, P. T. Calamia, and S. Nakanishi, "Frequency-domain edge diffraction for finite and infinite edges," *Acta Acustica united w Acustica*, vol. 95, pp. 568–572, 2009.

[11] H. Kuttruff, *Room Acoustics. Fifth edition.* CRC Press, 2014.

[12] F. Silva, P. Guillemain, J. Kergomard, B. Mallaroni, and A. N. Norris, "Approximation formulae for the acoustic radiation impedance of a cylindrical pipe," *Journal of Sound and Vibration*, vol. 322, pp. 255–263, 2009.

[13] W. Duan and R. Kirby, "A hybrid finite element approach to modeling sound radiation from circular and rectangular ducts," *Journal of the Acoustical Society of America*, vol. 131, pp. 3638–3649, 2012.